Electrochemical and spectroscopic properties of a series of *tert*-butyl-substituted *para*-extended quinones

Jinkui Zhou and Anton Rieker*

Institute of Organic Chemistry, University of Tübingen, Auf der Morgenstelle 18, D-72076, Tübingen, Germany

Six extended *para*-quinones 1–6 with sterically hindered keto groups have been characterized by UV–VIS, ^{1}H NMR and ^{13}C NMR spectroscopy. Their electrochemical properties were investigated in pyridine solution using cyclic voltammetry, differential pulse voltammetry, chronoamperometry and controlled-potential electrolysis. All species exhibit two successive one-electron reductions leading to the dianions *via* the monoanions; the dianions can be reoxidized to the quinones. An EE-type mechanism for 1–6 was verified by computer simulation; the standard rate constants (k_{s1} and k_{s2}) of the heterogeneous charge-transfer are in the region of 6.5–12.5 × 10^{-3} cm s^{-1}. The first reduction peak potentials show a good linear relationship with the calculated LUMO energy levels. The radical anions, prepared electrochemically in the first reduction step, were persistent for several hours in the absence of air. They were also characterized by UV–VIS, EPR and ENDOR spectroscopy revealing that the odd electron is delocalized over the whole π-system.

Introduction

Quinones are an important group of compounds in organic electrochemistry due to their multistep redox properties.[1] They also play a major role in the electron transfer chain of all living organisms.[2] For several years, there has been an increasing application of extended quinones as electron acceptors for the production of organic conducting materials.[3–7] Like quinones, their radical anions also have attracted interest in biology, medicine and chemistry.[1,8] Some benzoquinones, naphthoquinones and anthraquinones have been most thoroughly investigated by electrochemistry and spectroscopy.[9–12] However, there have been only a few reports referring to extended quinones like **1**–**6** which are assembled from two 3,5-di-*tert*-butyl-4-oxocyclohexa-2,5-dienylidene units separated by spacers SP prone to π-conjugation (see Table 1). The reduction potentials of **1** in MeCN [13,14a] and CH_2Cl_2,[14b] and that of **3** in dimethylformamide (DMF)[15] have been given, and the hyperfine splitting constants of the radical anion of **1** reported.[13] In this paper, a systematic comparative spectroscopic and electrochemical study of the quinones **1**–**6** is described. The electrochemical properties of **1**–**6** were investigated by cyclic voltammetry (CV), differential pulse voltammetry (DPV), chronoamperometry (CA) and controlled-potential electrolysis (CPE). These quinones and their radical anions were also characterized by spectroscopic methods, as UV–VIS, ^{1}H and ^{13}C NMR spectroscopy and EPR/ENDOR spectroscopy. In particular, the electrochemical properties of the extended quinones **1**–**6** and the EPR spectra of their anions should be influenced by the variation of the spacers (Sp) between the oxocyclohexadienylidene units, whereas the *tert*-butyl groups as well as the extended π-system should provide the necessary stability of the species in their different oxidation states.

Experimental

Instrumentation

Elemental analyses were performed in the microanalytical laboratory of our Institute using a Carlo Erba Elemental Analyzer-1106. IR spectra were recorded on a Perkin-Elmer 281 spectrometer (KBr pellets). UV–VIS spectra were measured on a Perkin-Elmer Lambda 5 UV–VIS spectrophotometer. NMR spectra were run on Varian A60, Bruker AC-250 and WM 400 spectrometers. All ^{1}H and ^{13}C chemical shifts are given relative to $SiMe_4$ as internal standard and for $CDCl_3$ as solvent; the coupling constants (*J*) are reported in Hz. Mass spectra were recorded with AEI MS9, Manchester, and Varian MAT instruments. EPR and ENDOR spectra were obtained with a Bruker ESP 300E spectrometer. For *g*-factor measurements, the field gradients were corrected by replacing the sample with a reference compound (2,6-di-*tert*-butyl-4-*tert*-butoxyphenoxyl in benzene, $g = 2.004\,63$).

Electrochemical experiments were carried out on a Windows-driven BAS 100W electro-chemical analyser (Bioanalytical Systems, Inc., West Lafayette, IN 47906, USA). For CV, DPV and CA a Pt disk electrode with an electroactive area of 0.068 cm^2 was used as working electrode. The auxiliary electrode consisted of a Pt wire. $Ag/AgClO_4$ (0.01 M in MeCN/0.1 M NBu_4PF_6) was used as reference electrode and separated by two glass frits from the Haber-Luggin capillary. All potentials given relate to this reference electrode. For CPE cylindrical Pt (10% iridium) gauze working and auxiliary electrodes, separated by a porous glass frit, were used. The commercial pyridine was purified by distilling it three times under argon after drying over KOH for several weeks, and then kept over 4 Å molecular sieves. Tetrabutylammonium hexafluorophosphate (NBu_4PF_6) as supporting electrolyte was prepared from tetra-butylammonium bromide and ammonium hexafluorophosphate, recrystallized four times from EtOH and dried *in vacuo* at 110 °C for 48 h.[16]

Computer simulations of CV-curves were accomplished with 'DigiSim 2.0' (Bioanalytical Systems, Inc., West Lafayette, IN 47906, USA).

AM1 semiempirical calculations were performed on a microcomputer using the SPARTAN program (Version 3.0, Wavefunction, Inc., Irvine, CA 92715, USA).

Synthesis

Quinones **1**,[17] **2b**,[20e] **3**,[18] **5**[19] and **6**[18] were prepared according to the references given. The synthesis of **4** will be described elsewhere.[20c]

Terphenoquinone **2a** was synthesized by us 30 years ago.[20a,20b] It has since been prepared by similar[7] and different[6] procedures. Since our earlier report has not been mentioned by these authors,[6,7] and since the mode of preparation and especially of purification of **2a** is crucial for the discussion of its

Table 1 Names and structures of extended *para*-quinones **1**–**6**

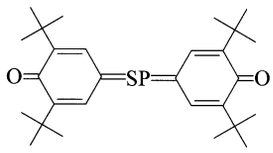

Compd.	SP	Name
1	═	3,3′,5,5′-Tetra-*tert*-butyl-4,4′-diphenoquinone
2a	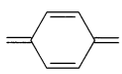	3,3″,5,5″-Tetra-*tert*-butyl-4,4″-*p*-terphenoquinone
2b	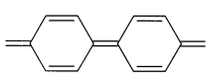	3,3‴,5,5‴-Tetra-*tert*-butyl-4,4‴-*p*-quaterphenoquinone
3	═CH—CH═	3,3′,5,5′-Tetra-*tert*-butyl-4,4′-stilbenequinone
4	═C(CN)—C(CN)═	2,3-Bis(3,5-di-*tert*-butyl-4-oxocyclohexa-2,5-dienylidene)succinonitrile
5	═CH—C(CN)═C(CN)—CH═	2,3-Bis(3,5-di-*tert*-butyl-4-oxocyclohexa-2,5-dienylidenemethyl)but-2-enedinitrile
6	═CH—N═N—CH═	1,2-Bis(3,5-di-*tert*-butyl-4-oxocyclohexa-2,5-dienylidenemethyl)diazene

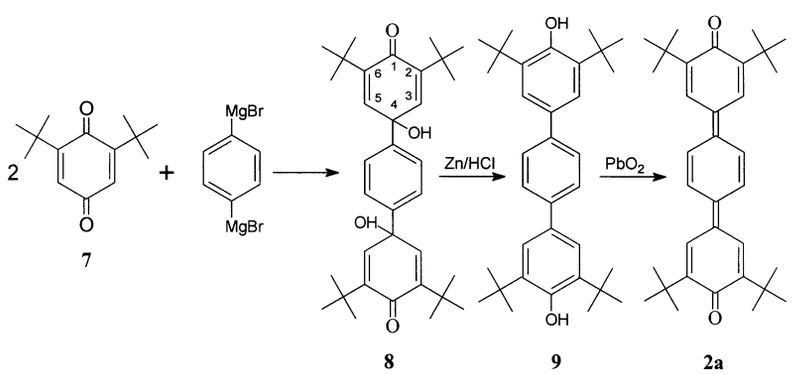

Scheme 1

paramagnetic behaviour, we give some details of our preparation (Scheme 1) hereafter.

4,4′-(1,4-Phenylene)bis[2,6-di-*tert*-butyl-4-hydroxycyclohexa-2,5-dien-1-one] 8. The bis-Grignard compound of 1,4-dibromobenzene in diethyl ether, prepared under N_2 and with exclusion of light, was added to 2,6-di-*tert*-butyl-*p*-benzoquinone **7** in diethyl ether (molar ratio 1,4-dibromobenzene : Mg : **7** = 1 : 2 : 2).[20a] The resulting yellow–brown precipitate was filtered after standing for 12 h and washed with diethyl ether. Afterwards, it was stirred with saturated aqueous ammonium chloride solution for 1 h, filtered by suction and washed with water. The product became violet at 100 °C and decomposed at 220 °C. It consisted of a mixture of the bisquinol **8** and 4-(4-bromophenyl)-2,6-di-*tert*-butyl-4-hydroxycyclohexa-2,5-dien-1-one, formed by the addition of 4-bromophenylmagnesium bromide, always present in the Grignard mixture, to **7**. By digestion with a large quantity of light petroleum (bp 50–70 °C) **8** remained, pure enough for reduction to **9** (see below).

Preparative TLC of the crude mixture on silica gel (Merck HF_{254}) with benzene–light petroleum (bp 50–70 °C)–acetone (45 : 50 : 5) (v/v/v), yielded pure **8** (10%), R_f 0.12, colourless crystals, mp 265 °C (from light petroleum) (Found C, 79.11; H, 9.10. $C_{34}H_{46}O_4$ requires C, 78.72; H, 8.94%). ν_{max}/cm^{-1} (KBr) 3484 (OH), 2941 (CH), 1653 (C=O), 1623 (C=O); δ_H(60 MHz, $CDCl_3$) 1.20 (36 H, s, Bu^t), 2.20 (2 H, br s, OH), 6.53 (4 H, s, H_{quinol}), 7.36 (4 H, s, H_{arom}); *m*/*z* (EI) 518 (M^+, 1%), 503 ($M^+ - 15$, 19), 502 ($M^+ - 18$, 49), 487 ($M^+ - 2 \times 15$, 99), 486 ($M^+ - 2 \times 16$, 100), 462 (49), 446 ($M^+ - 56$, 30), 406 ($M^+ - 2 \times 56$, 89), 405 (91).

3,3″,5,5″-Tetra-*tert*-butyl-*p*-terphenyl-4,4″-diol 9 and 3,3″,5,5″-tetra-*tert*-butyl-*p*-terphenoquinone 2a. The crude **8** obtained

in the previous experiment was reduced by Zn/HCl, as described for related quinols.[20d] The resulting **9** was oxidized without further purification: **9** (220 mg, 0.45 mmol) was stirred with PbO_2 (400 mg, 1.67 mmol) in benzene (40 ml) under N_2 for 1 h at 25 °C. The resulting deep violet solution was filtered from PbO_2, evaporated *in vacuo* and purified by TLC on silica gel (Merck HF_{254}) with benzene–light petroleum (bp 50–70 °C) (1 : 3) (v/v) to give **2a** (130 mg, 60% relative to crude **8**), R_f 0.21, and **9** (55 mg, 25% relative to crude **8**), R_f 0.37.

Compound 9. Faintly yellow plates, mp 290–291 °C (from light petroleum, bp 50–70 °C) (Found: C, 83.65; H, 9.47. $C_{34}H_{46}O_2$ requires C, 83.90; H, 9.53%). Since **9** is very sensitive towards oxygen, it is advisable to treat it in ethanolic solution with a small amount of sodium dithionite before recrystallisation. ν_{max}/cm^{-1} (KBr) 3597 (OH), 2941 (CH); λ_{max}/nm (MeOH) 293 (log ε 4.79), 222 (4.77); 245 (4.77); δ_H(60 MHz, $CDCl_3$) 1.47 (36 H, s, Bu^t), 5.02 (2 H, s, OH), 7.28 (4 H, s, H_{arom}), 7.43 (4 H, s, H_{arom}).

Compound 2a. Deep-green flakes (from diethyl ether), showing a metallic lustre and strongly light refractive. After digestion with light petroleum (bp 50–70 °C) and drying *in vacuo*, the crystals became violet at 213 °C and melted at 240–241 °C (decomp.) to a red–brown liquid. In solution, **2a** was always violet. (Found C, 83.95; H, 9.86. $C_{34}H_{44}O_2$ requires C, 84.25; H, 9.15%). ν_{max}/cm^{-1} (KBr) 2967 cm^{-1} (CH), 1572, 1530, (quinonoidal system); λ_{max}/nm (MeOH) 501 (log ε 5.25), 538 (5.45), 588 (sh, 4.21), 634 (4.06); ^{1}H and ^{13}C NMR see below; *m*/*z* (EI): 486 ($M^+ + 2$), for more details see ref. 20*b*.

NMR spectra of 1–6

All quinones investigated were characterized and checked for purity by their NMR spectra, which are given below. The assignments were made by chemical shifts consideration, intensities, coupling constants, H/H- and H/C-COSY spectra and by calculations using the ACD/CNMR program (Version 1.1). Assigments marked by asterisks may be exchanged. For simplicity the numbering system given below was chosen for the carbon atoms.

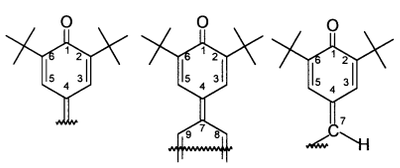

1 **2a** **3**

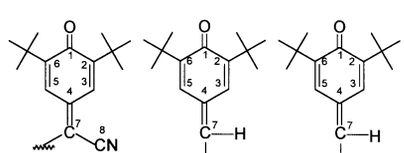

4 **5** **6**

1. δ_H(250.1 MHz; $CDCl_3$) 1.35 (36 H, s, Bu^t), 7.70 (4 H, s, 3,5-H); δ_C(62.9 MHz; $CDCl_3$) 29.60 (12 Me), 36.03 (4 Me_3C), 125.99 (4 C-3,5), 136.15 (2 C-4), 150.50 (4 C-2,6), 186.47 (2 C-1).

2a. δ_H(250.1 MHz; $CDCl_3$) 1.31 (36 H, s, Bu^t), 7.62 (4 H, s, 8,9-H), 7.74 (4 H, s, 3,5-H); δ_C(62.9 MHz; $CDCl_3$) 29.87 (12 Me), 36.18 (4 Me_3C), 125.65 (4 C-3,5), 127.51 (4 C-8,9), 134.56 (2 C-4*), 139.18 (2 C-7*), 149.71 (4 C-2,6), 186.06 (2 C-1).

3. δ_H(250.1 MHz; $CDCl_3$) 1.33 (18 H, s, Bu^t), 1.36 (18 H, s, Bu^t), 7.02 (2 H, d, *J* 2.4, H-3*), 7.24 (2 H, s, H-7), 7.52 (2 H, d, *J* 2.3, H-5*); δ_C(100.6 MHz; $CDCl_3$) 29.53 (6 Me), 29.60 (6 Me), 35.33 (2 Me_3C), 35.74 (2 Me_3C), 124.34 (2 C-3*), 133.30 (2 C-7), 134.09 (2 C-5*), 136.08 (2 C-4), 149.76 and 150.07 (4 C-2,6), 186.35 (2 C-1).

4. δ_H(250.1 MHz; $CDCl_3$) 1.26 (18 H, s, Bu^t), 1.34 (18 H, s, Bu^t), 7.10 (2 H, d, *J* 2.40, H-3*), 7.47 (2 H, d, *J* 2.4, H-5*); δ_C(62.9 MHz; $CDCl_3$) 29.47 (12 Me), 36.15 (2 Me_3C), 36.30 (2 Me_3C), 108.31 and 115.30 (2 C-7 and 2 C-8), 125.54 and 128.37 (2 C-3 and 2 C-5), 146.39 (2 C-4), 153.58 and 154.20 (2 C-3 and 2 C-6), 185.77 (2 C-1).

5. δ_H(250.1 MHz; $CDCl_3$) 1.31 (18 H, s, Bu^t), 1.34 (18 H, s, Bu^t), 6.91 (2 H, d, *J* 2.4, H-3*), 7.12 (2 H, s, H-7), 8.25 (2 H, d, *J* 2.5, H-5*); δ_C(100.6 MHz; $CDCl_3$) 29.55 (12 Me), 35.66 (2 Me_3C), 36.54 (2 Me_3C), 114.91 and 121.64 (2 C-8 and 2 C-9), 124.64 (2 C-3*), 130.58 (2 C-7), 134.18 (2 C-5*), 139.77 (2 C-4), 151.89 and 152.50 (2 C-2 and 2 C-6), 186.04 (2 C-1).

6. δ_H(250.1 MHz; $CDCl_3$) 1.33 (18 H, s, Bu^t), 1.35 (18 H, s, Bu^t), 7.13 (2 H, d, *J* 2.2, H-3*), 7.88 (2 H, s, H-7), 8.18 (2 H,d, *J* 2.1, H-5*); δ_C(100.6 MHz; $CDCl_3$) 29.90 (6 Me), 29.93 (6 Me), 36.05 (2 Me_3C), 36.21 (2 Me_3C), 126.93 and 131.94 (2 C-3 and 2 C-5), 138.73 (2 C-4), 150.92 and 152.78 (2 C-2 and 2 C-6), 154.02 (2 C-7), 186.84 (2 C-1).

Results and discussion

Electrochemical investigations

The cyclic voltammetric investigations of **1**–**6** were performed in pyridine solution containing 0.1 M Bu_4NPF_6 at room temperature under an argon atmosphere using the scan rate range 50–1000 mV s^{-1}. The experimental cyclic voltammograms of **2a** and **4**–**6** at a scan rate of 100 mV s^{-1} are shown in Fig. 1 (solid line), and the potential data of **1**–**6** are summarized in Table 2. All quinones **1**–**6** exhibited two well separated reduction peaks P_r^1, P_r^2 and two reoxidation peaks P_o^1, P_o^2. As can be seen from Table 2, the variation of the spacers (SP) between the oxocyclohexadienylidene units changes the redox potentials of **1**–**6**. The first reduction potentials (E_p^{r1}) become more negative in the order **5** < **4** < **6** < **2a** < **1** < **3**. This indicates that **2a**, **4** and **5** possess a higher electron-accepting ability than **1**, whereas **3** displays even a weaker electron-accepting ability than the reference quinone. The ΔE_p^r (= $E_p^{r2} - E_p^{r1}$) values for **1**, **4** and **5** are *ca*. 510, 400 and 370 mV, respectively, and much larger than those for **2a** (236 mV), **2b** (80 mV),[20e] **3** (274 mV) and **6** (300 mV), indicating a larger Coulomb repulsion in the dianion of the former than in the latter.[10b] The ΔE_p^r of *p*-extended 'phenoquinones' decreases in the order **1** > **2a** > **2b**, indicating that the longer the SP in this series, the smaller the Coulomb repulsion in the corresponding dianions. As a consequence of the differences in ΔE_p^r for **1**–**6**, E_p^{r2} becomes more negative in the order **5** < **6** < **2a** < **4** < **3** < **1**, which is different from that of E_p^{r1}.

With increasing scan rate both reduction and re-oxidation peak currents increased. The ratios of I_p^{o1}/I_p^{r1} and I_p^{o2}/I_p^{r2} for **1**–**6** were approximately 1.0 and independent of the scan rates. The currents of the reduction peaks (I_p^{r1}, I_p^{r2}) and re-oxidation peaks (I_p^{o1}, I_p^{o2}) proved to be diffusion-controlled at the platinum electrode because they depended linearly on the square root of the scan rate.[21]

The peak potentials of **1**–**6** are also influenced by the scan rate. With increasing scan rate, the first and the second reduction peaks (E_p^{r1} and E_p^{r2}) were shifted towards more negative potentials. In contrast, the first and the second reoxidation peaks (E_p^{o1} and E_p^{o2}) moved towards more positive potentials. Thus, the potential separations ΔE_p (= $E_p^o - E_p^r$) increased, and they could be used to measure the rate constants of the heterogeneous charge transfer (k_s).[22,23] The values of k_{s1} and k_{s2} obtained are shown in Table 3. For **2a** and **3**–**5**, ΔE_p^2 (= $E_p^{o2} - E_p^{r2}$) is approximately equal to ΔE_p^1 (= $E_p^{o1} - E_p^{r1}$), k_{s1} and k_{s2} are almost the same. However, in the case of **1**, ΔE_p^2 was found to be larger than ΔE_p^1, so k_{s2} is smaller than k_{s1}, *i.e*. the second electron transfer step is slower than the first one.

The differential pulse voltammograms of **2a**, **4**–**6** are shown

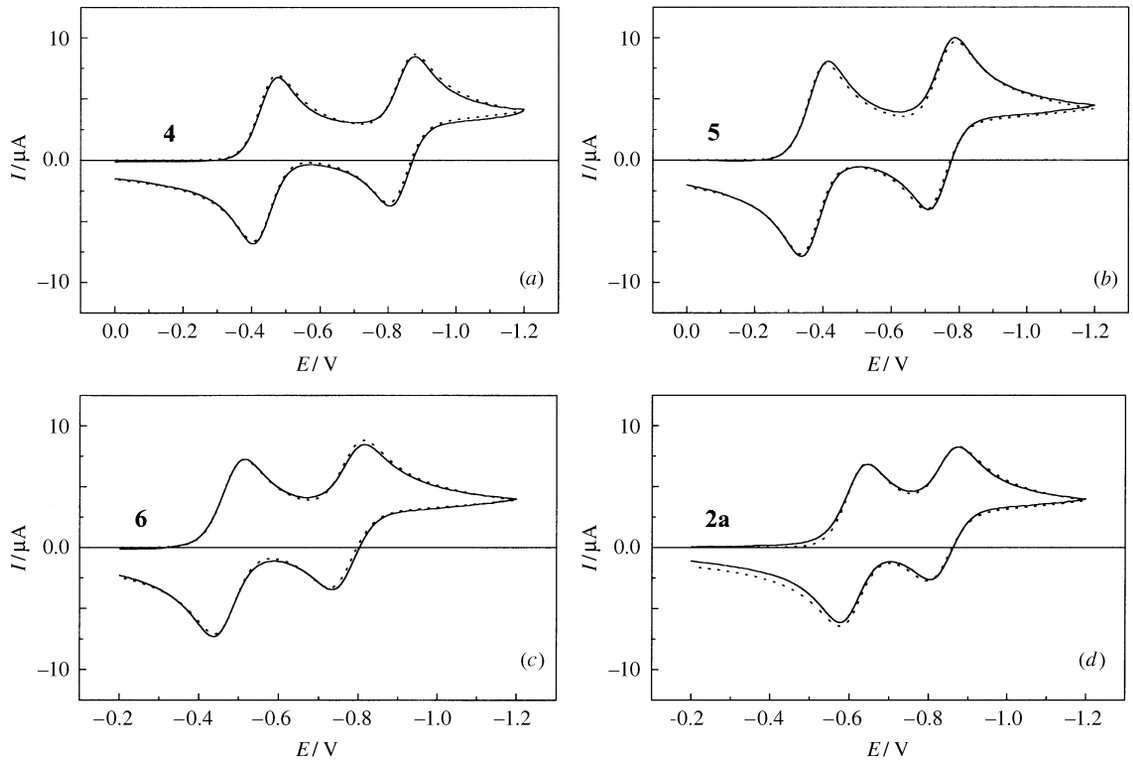

Fig. 1 Cyclic voltammograms of (0.6 mM) substrate in pyridine solution containing 0.1 M NBu_4PF_6 at room temperature; potential *vs*. $Ag/AgClO_4$ (0.01 M in MeCN/0.1 M NBu_4PF_6); scan rate, 100 mV s^{-1}; (*a*) **4**, (*b*) **5**, (*c*) **6**, (*d*) **2a**; (——) experiment, (· · · ·) simulation

Table 2 Peak potentials (E_p) and formal potentials (E^o)[a]

Compd	E_p^{r1}/mV	E_p^{o1}/mV	E^{o1}/mV	E_p^{r2}/mV	E_p^{o2}/mV	E_p^{o2}/mV
1	−863	−786	−828	−1371	−1272	−1322
2a	−648	−578	−613	−875	−804	−840
3	−970	−898	−934	−1244	−1168	−1206
4	−476	−405	−441	−878	−805	−842
5	−416	−339	−378	−786	−706	−748
6	−514	−438	−476	−814	−734	−774

[a] Potentials *vs*. Ag/(0.01 M) $AgClO_4$ electrode. E^o, the mean value of E_p^r and E_p^o.

Table 3 Rate constants of charge transfer and diffusion coefficents

Compd	$k_{s1}/10^{-3}$ cm s^{-1}	$k_{s2}/10^{-3}$ cm s^{-1}	$D/10^{-6}$ cm^2 s^{-1}
1	10.5	6.5	5.7
2a	12.3	12.0	4.6
3	11.9	11.4	5.3
4	11.8	11.2	5.1
5	11.5	11.1	4.9
6	10.5	10.0	5.0

in Fig. 2. The second reduction peak heights of **2a**, **3**–**5** are 5–10% smaller than the first ones; the reason for this might be that radical anions are negatively charged and could be repelled from the diffusion layer around the cathode into the bulk of the solution.[24] The ratio of I_p^{r2}/I_p^{r1} for **1** is only 0.75, resulting mainly from the above mentioned fact that k_{s1} is smaller than k_{s2}.[25,26]

Controlled-potential electrolysis was carried out to determine the number of electrons involved in the electrochemical steps. If the potential, chosen according to CV, was set between E_p^{r1} and E_p^{r2}, **1**–**6** should be reduced in the first step to the radical anions, and, indeed, one electron was consumed per molecule. If the potentials chosen were 200 mV more negative than the second reduction peak potentials, the number of electrons transferred in the reduction process was found to be two per molecule for **1**–**6**, as expected for a reduction of the quinone to the dianion state.

Chronoamperometry has proved to be very useful for the measurement of diffusion coefficients of electroactive substances and for the explanation of the mechanism of charge transfer.[21] The diffusion coefficients of **1**–**6** were determined in pyridine solution containing 0.1 M NBu_4PF_6 according to the Cottrell equation [eqn. (1)] (*i*, current; *n*, number of electrons

$$i = nFAcD^{\frac{1}{2}}/\pi^{\frac{1}{2}}\, t^{\frac{1}{2}} \qquad (1)$$

exchanged per molecule, determined by CPE; *F*, Faraday's constant; *A*, electrode surface area; *c*, concentration of compound; *D*, diffusion coefficient; *t*, time from initiation of the step). A plot of *i vs*. $1/t^{\frac{1}{2}}$ transforms the data into a linear relation whose slope (*k*) is $nFAcD^{\frac{1}{2}}/\pi^{\frac{1}{2}}$. The applied potential E_i (initial potential, where no electrolysis occurs) and E_f (final potential, where electrolysis is complete) were chosen according to the CV (Fig.1, Table 2). The diffusion coefficients measured are shown in Table 3. CA could also be used to confirm if a chemical step occurred between two electron transfer steps, because the slope should be proportional to the number of electrons transferred in the electrochemical process. If the E_f values were chosen between E_p^{r1} and E_p^{r2}, the slopes were only about half of those obtained with E_f values, which were more negative than E_p^{r2}. Therefore, it can be concluded that **1**–**6** are reduced to anions in the first step, then the anions are reduced to dianions without a chemical step between the first and second electron transfer.[21]

From the structures of **1**–**6** and the experimental results of

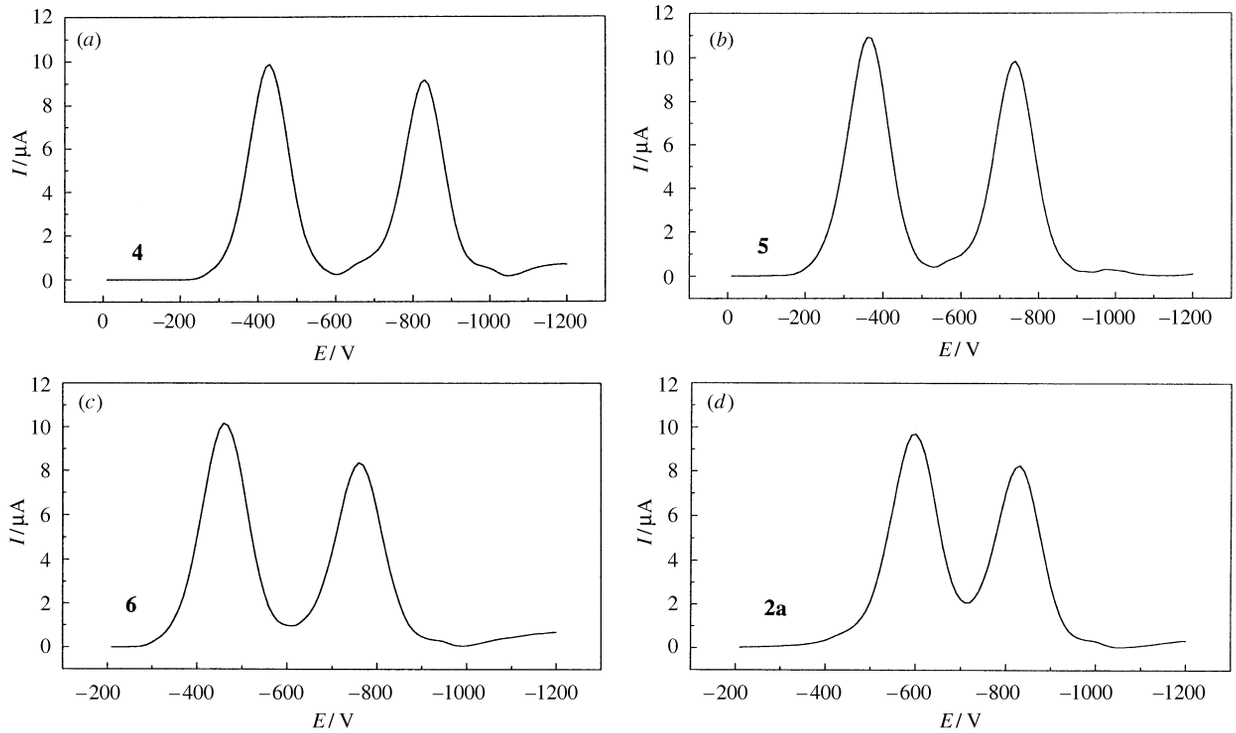

Fig. 2 Differential pulse voltammograms of (0.6 mM) substrate in pyridine solution containing 0.1 M NBu_4PF_6; potential *vs.* $Ag/AgClO_4$ (0.01 M in MeCN/0.1 M NBu_4PF_6); scan rate, 20 mV s^{-1}; pulse amplitude, 50 mV; pulse width, 50 ms; pulse period, 200 ms; (*a*) **4**, (*b*) **5**, (*c*) **6**, (*d*) **2a**

CV, CA and CPE measurements the following reduction mechanism can be derived: each species is reduced in the first step by a one-electron transfer to form persistent radical anions (which can further be characterized by EPR and ENDOR spectroscopy, see below). The radical anions are reoxidized to the quinone state or further reduced in a second one-electron transfer to dianions. The latter are reoxidizable in two successive one-electron transfers up to the quinone state. Therefore, the reduction mechanism of **1**–**6** can be denoted as a quasi-reversible EE process [eqns. (2) and (3)].

$$Q \underset{k_{s1}}{\overset{e^-}{\rightleftharpoons}} Q^{\bullet -} \quad E^{o1} \tag{2}$$

$$Q^{\bullet -} \underset{k_{s2}}{\overset{e^-}{\rightleftharpoons}} Q^{\bullet =} \quad E^{o2} \tag{3}$$

In order to get further verification of the experimentally confirmed EE processes, a computer simulation was carried out. Fig.1 shows the excellent agreement between simulated (dotted line) and experimental CV curves (solid line). The simulated parameters, such as formal potentials and rate constants of the heterogeneous charge transfer, are the same as those in Tables 2 and 3, obtained from the experimental results. The charge transfer coefficients, α, obtained theoretically, lie between 0.47 and 0.53.

Besides two conjugated C=O bonds, the species **4**–**6** contain also reducible −N=N− or −C≡N bonds. However, their reduction features are similar to those of **1** and **2a**, indicating that the reduction of these multiple bonds can only take place at a potential beyond the reduction of the solvent. Hence, it was not observed under our experimental conditions.

Correlation between first reduction potentials and MO energy levels

As shown in Fig. 3, the first reduction potentials of **1**–**6** exhibit a good linear relationship ($r = 0.980$) with LUMO energy levels obtained by the AM1 molecular orbital calculation. This is expected for the monovalent reduction to the radical anions, whereby one electron is transferred into the LUMO.

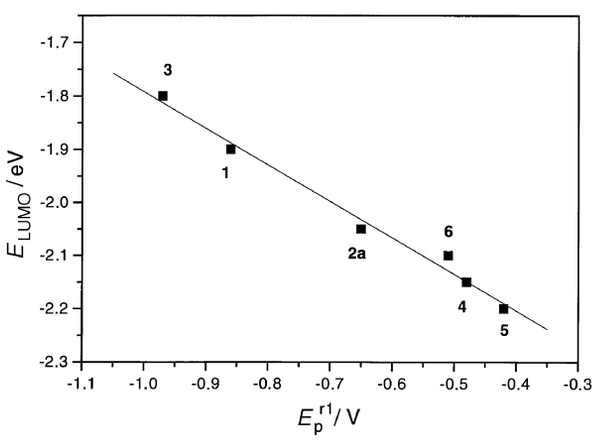

Fig. 3 Plot of E_p^{r1} *vs.* LUMO energy, E_p^{r1} obtained from Table 2

Spectroscopic investigations

The variation of the spacers (SP) between the oxocyclohexadienylidene units of the extended quinones **1**–**6** should not only influence the electrochemical behaviour, but also the spectroscopic properties of these extended quinones and their radical anions. UV–VIS, EPR and ENDOR spectroscopic experiments were therefore carried out to characterize **1**–**6** and their radical anions (^{1}H NMR and ^{13}C NMR data of **1**–**6** are given in the experimental section).

UV–VIS spectroscopy. In their electronic spectra, **1**–**6** and their radical anions exhibit intense absorption maxima in the visible region (see Fig. 4 for **4**/**4**$^{\bullet -}$ and **5**/**5**$^{\bullet -}$). The maximum absorption wavelengths (λ_{max}) and extinction coefficients (log ε) are summarized in Table 4. The yellow **1**, **4** and orange **3** showed only one absorption maximum in the range 415–460 nm, while red **5**, **6** and blue **2a** exhibit two absorption maxima in the range 470–550 nm. When **1**–**6** were electrochemically reduced to the radical anions, colour changes were observed. Each radical anion showed only one absorption peak, and the λ_{max} was shifted bathochromically. The green anion radicals **3**$^{\bullet -}$–**6**$^{\bullet -}$ reveal remarkable differences in the absorption maxima as compared to those of the parent compounds **3**–**6**, $\Delta\lambda_{max}$

Table 4 λ_{max} of **1**–**6** and **1**$^{\bullet -}$–**6**$^{\bullet -}$

Compd	λ_{max}/nm (log ε)	Radical anion	λ_{max}/nm (log ε)
1	430 (4.67)	**1**$^{\bullet -}$	482 (4.54)
2a	510 (4.42), 550 (4.84)	**2a**$^{\bullet -}$	580 (4.56)
3	460 (4.81)	**3**$^{\bullet -}$	611 (4.67)
4	415 (4.41)	**4**$^{\bullet -}$	710 (4.38)
5	481 (4.64), 515 (4.82)	**5**$^{\bullet -}$	651 (4.75)
6	470 (4.72), 510 (4.75)	**6**$^{\bullet -}$	617 (4.71)

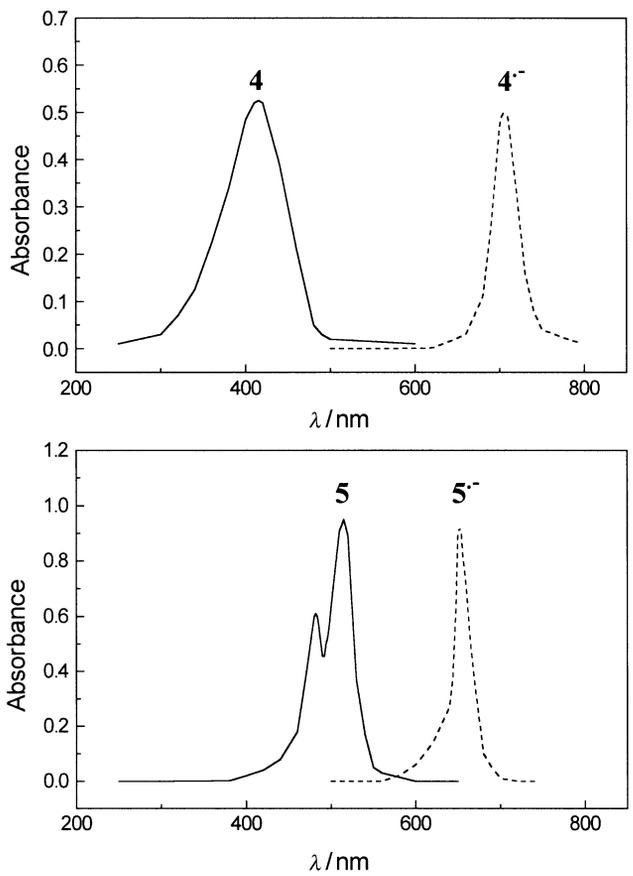

Fig. 4 UV–VIS spectra of **4**, **5** (——) and **4**$^{\bullet -}$, **5**$^{\bullet -}$ (– – – –)

being *ca*. 110–300 nm. On the other hand, the colour change of **1** from yellow to orange and that of **2a** from blue to green–blue on reduction corresponds only to small changes in the absorption maxima. As expected, the UV spectra of the dianions reveal strong hypsochromic shifts, because here the rings are essentially aromatic.

EPR and ENDOR spectroscopy. The radical anions **1**$^{\bullet -}$–**6**$^{\bullet -}$ were generated by electrochemical reduction in pyridine solution at room temperature and proved to be persistent for several hours in the absence of air as shown by EPR investigation. The EPR spectra obtained at room temperature are presented in Fig. 5. Each spectrum appeared in the $g = 2.005$ region, where the EPR spectra of radical anions of quinones are usually observed. The hyperfine splitting constants (hfs) a_H and g tensor values are listed in Table 5. The hyperfine structures of the spectra are caused by interaction of the odd electron with the protons of the oxocyclohexadienylidene units *and* of the spacer. The interaction with the protons of the *tert*-butyl groups could not be resolved by EPR spectroscopy. In addition, ENDOR spectroscopy was carried out to characterize the radical anions **1**$^{\bullet -}$–**6**$^{\bullet -}$. As shown in Fig. 6, the ENDOR spectra at 333 K allow the resolution of the different proton couplings. The interaction of the odd electron with the protons of the *tert*-butyl groups has also been resolved by ENDOR spectroscopy. The coupling constants (a_H) obtained at 333 K from ENDOR

Table 5 a_H and g values of radical anions (1 G = 10^{-4} T)

Radical anion	a_H/G			g value
1$^{\bullet -}$	0.45[a], 0.46[b]		0.05[e]	2.004 66
2a$^{\bullet -}$	0.20[a], 0.19[b]	0.75[c], 0.72[d]	0.05[e]	2.005 00
3$^{\bullet -}$	0.28[a], 0.30[b]	1.85[c], 1.89[d]	0.04[e]	2.005 03
4$^{\bullet -}$	0.30[a], 0.33[b]		0.06[e]	2.005 95
5$^{\bullet -}$	0.45[a], 0.46[b]	0.94[d], 1.01[f]	0.04[e]	2.004 90
6$^{\bullet -}$	0.47[a], 0.46[b]	0.48[c], 0.46[d]	0.04[e]	2.004 81

[a] Quinonoid proton, obtained by EPR spectroscopy at room temperature. [b] Quinonoid proton, obtained by ENDOR at 333 K. [c] Bridge proton, obtained by EPR at room temperature. [d] Bridge proton, obtained by ENDOR at 333 K. [e] *tert*-Butyl proton. [f] Bridge proton, obtained by simulation.

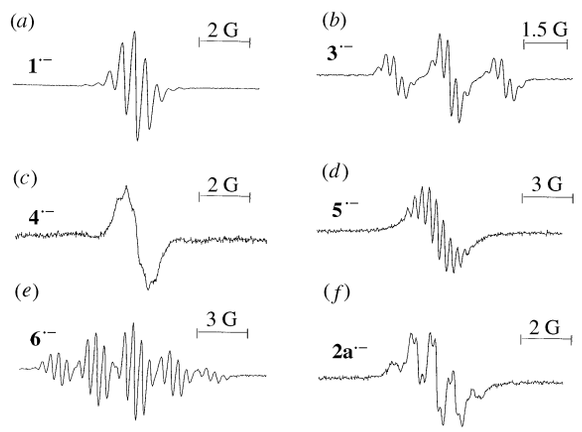

Fig. 5 EPR spectra of the radical anions in pyridine solution at 298 K (*a*) **1**$^{\bullet -}$, (*b*) **3**$^{\bullet -}$, (*c*) **4**$^{\bullet -}$, (*d*) **5**$^{\bullet -}$, (*e*) **6**$^{\bullet -}$, (*f*) **2a**$^{\bullet -}$

spectra are approximately equal to those obtained at room temperature with EPR spectroscopy (Table 5).

The EPR spectrum of **1**$^{\bullet -}$ consists of five lines with the relative intensities 1:4:6:4:1, demonstrating an equal coupling of the delocalized odd electron to four aromatic protons with $a_H = 0.45$ G, close to the value of 0.46 G, determined for electrochemically produced **1**$^{\bullet -}$ in CH_3CN solution.[12] Smaller signals at both wings may be due to ^{13}C couplings. Since **4**$^{\bullet -}$ contains the same ring proton system as **1**$^{\bullet -}$, a hfs of five lines is also expected here and could be observed, although the resolution is poor, probably due to a small additional but unresolved coupling with the ^{14}N nuclei [Fig. 5(*c*)]. The ENDOR spectra of **1**$^{\bullet -}$ and **4**$^{\bullet -}$, without bridge protons in both species, therefore exhibit only two similar line pairs due to the coupling of the odd electron with the quinonoid protons (0.44 and 0.33 G, respectively) and with the *tert*-butyl protons (50–60 mG).

The stilbenequinone anion **3**$^{\bullet -}$ exhibits a triplet hfs with $a_H = 1.85$ G, caused by the two equivalent methine protons of the spacer. Each triplet line is further split into a quintet with $a_H = 0.28$ G by the four quinone ring protons [Fig. 5(*b*)]. As a consequence, the ENDOR spectrum of **3**$^{\bullet -}$ contains one more line pair ($a_H = 1.89$ G), when compared to that of **1**$^{\bullet -}$. The other two pairs again correspond to the coupling of the free electron with the quinone ring protons ($a_H = 0.30$ G) and *tert*-butyl protons ($a_H = 0.04$ G).

As shown in Fig. 5(*d*), **5**$^{\bullet -}$ gives rise to a hfs of 11 lines ($a_H = 0.45$ G). The pattern thus, is, completely different from that of **3**$^{\bullet -}$, although the number of protons is the same. A straightforward assignment from the EPR spectrum is not possible. Presumably, as in the case of **4**$^{\bullet -}$, a small coupling of the free electron with the ^{14}N nuclei of the two nitrile groups is complicating the spectrum. Anyway, the coupling of the methine spacer protons must be much smaller than in **3**$^{\bullet -}$, which is confirmed by the ENDOR spectrum [Fig. 6(*d*)], showing the largest $a_H = 0.94$ G, which is assigned to the methine

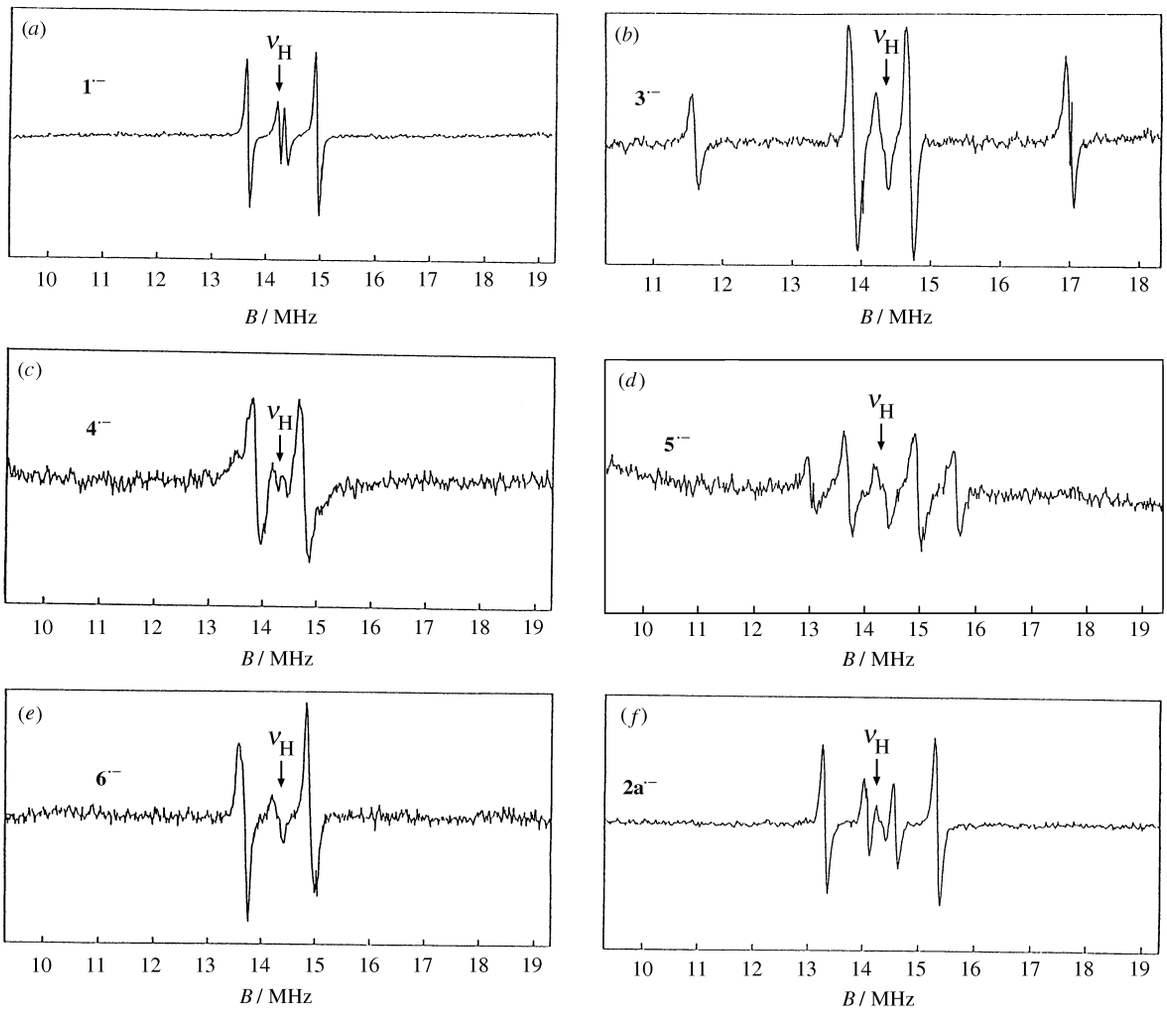

Fig. 6 ENDOR spectra of the radical anions in pyridine solution at 333 K (*a*) $\mathbf{1}^{\bullet-}$, (*b*) $\mathbf{3}^{\bullet-}$, (*c*) $\mathbf{4}^{\bullet-}$, (*d*) $\mathbf{5}^{\bullet-}$, (*e*) $\mathbf{6}^{\bullet-}$, (*f*) $\mathbf{2a}^{\bullet-}$

protons, besides $a_H = 0.46$ G (quinonoid ring protons) and $a_H = 0.04$ G (Bu^t protons). A simulation of the EPR spectrum using the ENDOR values gives 11 lines, which agrees with the experimental results.

The EPR spectrum of $\mathbf{6}^{\bullet-}$ [Fig. 5(*e*)] reveals a large (2.1 G) quintet splitting (1:2:3:2:1), resulting from the interaction of the odd electron with the two equivalent nitrogen nuclei. Each quintet line is further split into a septet ($a_H = 0.45$ G), of which only the five central lines are clearly resolved due to partial overlapping of the wings. This means that the four quinonoid ring protons and the two methine spacer protons are *de facto* equivalent. This is further confirmed by simulation and by the ENDOR spectrum [Fig. 6(*e*)], showing only two resolved line pairs.

The terphenoquinone anion $\mathbf{2a}^{\bullet-}$ [Fig. 5(*f*)], finally, exhibits a quintet with $a_H = 0.75$ G, resulting from the coupling with the two spacer protons, which is further split into a poorly resolved quintet, due to the coupling with the quinonoid ring protons ($a_H = 0.20$ G). This is again confirmed by the ENDOR spectrum [Fig. 6(*f*)]. The ENDOR spectrum of $\mathbf{2a}^{\bullet-}$ is identical with a spectrum reported by Boldt *et al.*[7] for the radical anion obtained by chemical reduction of **2a** by potassium in 1,2-dimethoxyethane, whereas the resolution of the EPR spectrum of the electrochemically prepared $\mathbf{2a}^{\bullet-}$ [Fig. 5(*f*)] is better than the reported one,[7] which showed only the larger quintet pattern.

There is another peculiarity to be discussed. West *et al.*,[6] as well as Boldt *et al.*,[7] reported that **2a** itself produces no EPR signal which means that this species is not in equilibrium with its biradical form, contrary to **2b**.[20e] On the other hand, the latter authors[7] assume some biradical 'character' for **2a** as 'indicated by the low frequency of ν(CO) (1575 cm^{-1}) which approaches that of phenoxy radicals (1560 cm^{-1})'. They express this by writing the resonance double arrow ⟷ between the quinonoid and biradical structure of **2a**. Owing to the multiplicity rule this would imply that the biradical in that case is a singlet ('antiferromagnetic' coupling), which would be in agreement with the EPR silence. For our samples of **2a** in benzene solution we could find a weak EPR signal; the corresponding radical concentration amounts up to 0.05% (determined against diphenyl picrylhydrazyl as reference radical).[20a] The EPR signal of this radical seems to be identical with the EPR signal obtained by Boldt *et al.*[7] on photolysis of **2a** in THF at 313 nm, outside the absorption region of **2a**, or by the oxidation of **9** with dichlorodicyanobenzoquinone (DDQ) in toluene, for example. The signal was ascribed to $\mathbf{2a}^{\bullet-}$, protonated at one oxygen, *i.e.* to the mono-phenoxyl radical of **9**. However, the signal is nearly identical also to the EPR signal of 4-(bromophenyl)-2,6-di-*tert*-butylphenoxyl,[20a,20d] which might be formed from 4-bromophenyl-2,6-di-*tert*-butylphenol by oxidation or irradiation. The latter phenol could be present as impurity in **9**, formed by reduction of 4-(4-bromophenyl)-2,6-di-*tert*-butyl-4-hydroxycyclohexa-2,5-dien-1-one, the addition product of the mono-Grignard compound of 1,4-dibromobenzene to quinone **7** (see Experimental part under synthesis of **8**). Hence, this 4-bromophenylphenol may also be present in **2a** and form the corresponding 4-bromophenylphenoxyl under irradiation. Indeed, Boldt *et al.*[7] do not give an elemental analysis of **8**, and for **9** and **2a** the found carbon values are too low. Also in our case, the found carbon values are at the lower border; however, due to our TLC purification process of the oxidized **9**, described in the Experimental section, **2a** ($R_f = 0.21$) could be safely separated from 4-(4-bromophenyl)-2,6-di-*tert*-butyl-

phenoxyl ($R_f = 0.25$). Therefore, the EPR signal observed by us in solutions of **2a** and by Boldt *et al.*[7] after the irradiation of **2a** almost certainly is due to the protonated semiquinone **2a**$^{\bullet -}$.

Conclusions

The electrochemical investigation of **1**–**6** revealed two successive one-electron reductions according to a quasi-reversible EE mechanism which could be confirmed experimentally and by simulation. The standard rate constants of the heterogeneous electron transfer ($k_{s1} = 10.5 \times 10^{-3}$–$12.3 \times 10^{-3}$ cm s^{-1}; $k_{s2} = 6.5 \times 10^{-3}$–$12 \times 10^{-3}$ cm s^{-1}) are of the usual dimension for a platinum electrode. The charge transfer coefficients were also determined by simulation and lie between 0.47 and 0.53. The electrochemical properties of **1**–**6** depend on the type of the spacer (SP) connecting the oxocyclohexadienylidene units. Cyano groups in the spacer shift both redox potentials to more positive values; especially **5** can be considered as a modified tetracyanoethene [the first reduction potential of tetracyanoethylene is −0.20 V *vs.* Ag/(0.1 M) $AgNO_3$ in CH_3CN],[27] with a less positive redox potential. The conjugated system is, however, much more extended in **5** than in TCE, which gives rise to very stable quinhydrones with the corresponding partially reduced forms (for more details see ref. 19).

The longer the extension of the π-system, the more bathochromically shifted are the UV maxima of **1**–**6** and of the corresponding anions, with the anions always showing a wavelength absorption longer than that of the parent quinones. This is especially evident with **4** ⟶ **4**$^{\bullet -}$, where a shift from 415 ⟶ 720 nm occurs, and the area of the so-called IR dyes is nearly reached.

The first reduction potentials of **1**–**6** exhibit a good linear relationship with the calculated LUMO energy levels. This, as well as EPR and ENDOR spectroscopy of the radical anions, demonstrates a delocalization of the odd electron over the whole conjugated system in **1**$^{\bullet -}$–**6**$^{\bullet -}$. The coupling constants of the free electron with protons may be regarded as spin probes and give some information on the spin densities of the free electron at the corresponding carbon atoms. The coupling constants of the *tert*-butyl and quinonoid ring protons do not change very dramatically in passing from **1**$^{\bullet -}$ to **6**$^{\bullet -}$. Only in the case of **2a**$^{\bullet -}$, as compared to **1**$^{\bullet -}$, the *a* value is decreasing to *ca.* 45%, because the planar cyclohexadienylidene spacer houses a high part of the free spin density. Also the stilbenequinone anion **3**$^{\bullet -}$ reveals a large coupling with the spacer protons, whereas in **5**$^{\bullet -}$ these protons couple much less. This may be due to a larger influence of conformational effects in **5**$^{\bullet -}$ (twisting around the spacer single bonds). A detailed discussion would, however, require the knowledge of the signs and the size of the free spin densities at all carbon, oxygen and nitrogen atoms of the molecular frame.

The quinones **1**–**6** may be useful as electron acceptors, and further work to test their ability to form charge transfer complexes is in progress.

Acknowledgements

We thank the Volkswagenstiftung (I/71009) and the Land Baden-Württemberg for support of this work. We also thank Dr Thomas Grösser, Tübingen, for the MO calculations.

References

1 J. Q. Chambers, in *The Chemistry of the Quinonoid Compounds*, (*a*) ed. S. Patai, Wiley, London, 1974, p. 737; (*b*) eds., S. Patai and Z. Rappoport, Wiley, Chichester, vol. II, 1988, p. 719.
2 D. Voet and J. G. Voet, *Biochemistry*, Wiley, New York, 1995.
3 H. Vogler and M. C. Böhm, *Theor. Chim. Acta*, 1984, **66**, 51.
4 Mc. R. Maxfield, A. N. Bloch and D. O. Cowan, *J. Org. Chem.*, 1985, **50**, 1789.
5 Y. Yamaguchi and M. Yokoyama, *Materials*, 1991, 3.
6 R. West, J. A. Jorgensen, K. L. Stearly and J. C. Calabrese, *J. Chem. Soc., Chem. Commun.*, 1991, 1234.
7 P. Boldt , D. Bruhnke, F. Gerson , M. Scholz, P. G. Jones and F. Bär, *Helv. Chim. Acta*, 1993, **76**, 1739.
8 J. Schreiber, C. Mottley, B. K. Binha, B. Kalyanaraman and R. P. Mason, *J. Am. Chem. Soc.*, 1987, **109**, 348.
9 (*a*) T. H. Jozefiak and L. L. Miller, *J. Am. Chem. Soc.*, 1987, **109**, 6560; (*b*) T. H. Jozefiak, J. E. Almlöf, M. W. Feyereisen and L. L. Miller, *J. Am. Chem. Soc.*, 1989, **111**, 4105; (*c*) J. E. Almlöf, M. W. Feyereisen, T. H. Jozefiak and L. L. Miller, *J. Am. Chem. Soc.*, 1990, **112**, 1206; (*d*) S. F. Rak and L. L. Miller, *J. Am. Chem. Soc.*, 1992, **114**, 1388.
10 (*a*) L. Echeverria, M. Delgado, V. J. Gatto, G. W. Gokel and L. Echegoyen, *J. Am. Chem. Soc.* 1986, **108**, 6825; (*b*) D. A. Gustowski, M. Delgado, V. J. Gatto, L. Echegoyen and G. W. Gokel, *J. Am. Chem. Soc.*, 1986, **108**, 7553; (*c*) D. A. Gustowski, M. Delgado, V. J. Gatto, L. Echegoyen and G. W. Gokel, *Tetrahedron Lett.*, 1986, **27**, 3487; (*d*) M. Delgado, D. A. Gustowski, H. K.Yoo, V. J. Gatto, G. W. Gokel and L. Echegoyen, *J. Am. Chem. Soc.* 1988, **110**, 119; (*e*) L. Echegoyen, Y. Hafez, R. C. Lawson, J. de Mendoza and T. Torres, *J. Org. Chem.*, 1993, **58**, 2009; (*f*) L. Echegoyen, R. C. Lawson, C. Lopez, J. de Mendoza, Y. Hafez and T. Torres, *J. Org. Chem.*, 1994, **59**, 3814.
11 H. Bock, P. Dickmann and H.-F. Herrmann, *Z. Naturforsch., Teil B*, 1991, **46**, 326.
12 B. Illescas, N. Martin, J. L. Segura, C. Seoane, E. Orti, P. M. Viruela and R. Viruela, *J. Org. Chem.*, 1995, **60**, 5643.
13 J. Petránek, J. Pilař and O. Ryba, *Coll. Czech. Chem. Commun.*, 1970, **35**, 2571.
14 (*a*) K. Takahashi and T. Suzuki, *J. Am. Chem. Soc.*, 1989, **111**, 5483; (*b*) K. Takahashi, T. Suzuki, K. Akiyama, Y. Ikegami and Y. Fukazawa, *J. Am. Chem. Soc.*, 1991, **113**, 4576.
15 M. O. F. Goulart and J. H. P. Utley, *J. Org. Chem.*, 1988, **53**, 2520.
16 J. Salbeck, Ph.D. Thesis, University of Regensburg, 1988, p. 200.
17 K. Ley, E. Müller, R. Mayer and K. Scheffler, *Chem. Ber.*, 1959, **92**, 2670.
18 A. Rieker and H. Kessler, *Tetrahedron*, 1968, **24**, 5133.
19 E. Müller, H.-D. Spanagel and A. Rieker, *Liebigs Ann. Chem.*, 1965, **681**, 141.
20 (*a*) O. Weiss, *Ingenieurarbeit*, Isny-Tübingen, 1967; (*b*) J. Heiss, K.-P. Zeller and A. Rieker, *Org. Mass Spectrom.*, 1969, **2**, 1325; (*c*) A. Rieker, M. El-Mobayed, A. Neumayer and W. Hiller, to be published; (*d*) A. Rieker and K. Scheffler, *Liebigs Ann. Chem.*, 1965, **689**, 78; (*e*) A. Rebmann, J. Zhou, P. Schuler, H. B. Stegmann and A. Rieker, *J. Chem. Res.*, (*S*), 1996, 318; (*M*), 1996, 1765.
21 P. T. Kissinger and W. R. Heineman, *Laboratory techniques in electroanalytical chemistry*, Marcel Dekker, New York, 1984, pp. 51–128.
22 R. S. Nicholson, *Anal. Chem.*, 1965, **37**, 1351.
23 J. Heinze, *Angew. Chem.*, 1984, **96**, 823.
24 S. Wawzonek, R. Berkey, E. W. Blaha and M. E. Runner, *J. Electrochem. Soc.*, 1956, **103**, 456.
25 A. M.Bond, *Modern Polarographic Methods in Analytical Chemistry*, Marcel Dekker, New York and Basel 1980, pp. 236–270.
26 G. C. Barker and A. W. Gardner, *At. Energ. Res. Estab.* (Brit) AERE Harwell, C/R, 1958, 2297.
27 J. E. Mulvaney, R. J. Cramer and H. K. Hall, Jr, *J. Polym. Sci., Chem. Ed.*, 1983, **21**, 309.

Paper 6/07113J
Received 18*th October* 1996
Accepted 20*th January* 1997